Interference and non-Franck-Condon effects in ionization of H_2 molecules by photon impact

To cite this article: O A Fojón *et al* 2011 *J. Phys.: Conf. Ser.* **288** 012025

View the article online for updates and enhancements.

Interference and non-Franck-Condon effects in ionization of H$_2$ molecules by photon impact

O. A. Fojón[1], J. Fernández[2], A. Palacios[2] and F. Martín[2]

[1]Instituto de Física Rosario (CONICET-UNR) 2000 Rosario, Argentina
[2]Departamento de Química C-9, Universidad Autónoma de Madrid, 28049 Madrid, Spain

E-mail: `fojon@ifir-conicet.gov.ar`

Abstract. We analyze theoretically interference effects in the spectra of electrons emitted in the H$_2$ photoionization by high energy linearly polarized photons. Molecular bound and continuum states are accurately described by means of B-spline basis allowing the inclusion of the nuclear degrees of freedom. One interesting feature is observed: the usual Franck-Condon behavior is not followed when the H$_2$ internuclear axis is parallel to the polarization direction. Moreover, this is related to the fact that for this molecular orientation and under certain conditions, the electron cannot be emitted in the direction of the radiation field. On the contrary, for H$_2$ molecules perpendicular to the polarization direction, the angular distribution of electrons is analogous to the one observed in the two slits Young's experiment.

1. Introduction

Nowadays, the study of interference effects in the electronic emission from diatomic molecules is a very active subject of research (see for instance [1]). In the sixties, Cohen and Fano explained anomalies in the photoelectron spectra of diatomic molecules [2]. They argued that the coherent emission from both molecular centers produced interferences when the de Broglie wavelength of the ejected electrons is of the order of the internuclear distance of the molecule in analogy with the Young's two slit experiment. They elaborated a simple model based on the following assumptions: i) ionization is basically a *one*-electron process, ii) the lowest molecular orbital ψ_g is well described in the Linear combination of atomic orbitals (LCAO) approximation ($\psi_g \sim 1s_A + 1s_B$, where $1s_A$ and $1s_B$ are atomic orbitals centred in nucleus A and B, respectively) and iii) the ionized electron is well described by a single-centre plane wave. In this way, Cohen and Fano showed that the total photoionization cross section is given by the analytical form

$$\sigma = \sigma_H \left[1 + \sin(k_e R)/(k_e R) \right] /(1 + S) \tag{1}$$

where σ_H is the photoionization cross section of a hydrogen atom with effective charge Z_{eff}, R is the equilibrium internuclear distance, S is the overlap between $1s_A$ and $1s_B$, and k_e is the electron wave vector. This formula shows the typical oscillatory behaviour associated with interferences.

However, it was not until recently that this kind of interference was experimentally detected in the differential cross sections of ionization of diatomic molecules by heavy ion impact [3]. The detection of these effects is not an easy task as the cross section as a function of the energy decreases quickly. In order to circumvent this inconvenient in those experiments, the ratio

between molecular cross sections and adequate atomic cross sections (two isolated atoms for instance, for which no interferences are produced) was considered. The coherent emission was then traced by analyzing oscillations in the mentioned ratios. In the same way, interferences effects were observed subsequently in the case of electronic impact [4, 5]. Moreover, the case of photoionization of hydrogen molecules was revisited in order to provide a realistic description of the photoionization spectra including the influence of the nuclear motion. In this work we review some of the remarkable results obtained for the case of impact of linearly polarized photons on hydrogen molecules. The Cohen and Fano predictions were studied concluding that they are valid at high emission energies. At low energies, deviations are observed mainly due to the electronic correlation and the nature of the molecular potential [6]. Interestingly, it was also observed that the usual Franck-Condon behavior is not followed when the H_2 internuclear axis is parallel to the polarization direction for linear polarized photons [7]. The origin of this anomaly may be related to interference and confinement effects [8]. Such effects are more easily evidenced in the electron angular distributions associated with specific vibrational states of the residual H_2^+ ion. For H_2 molecules oriented perpendicular to the polarization direction, the distributions are close to the ones obtained in the Young's double-slit experiment. In the case of molecules parallel to the polarization direction and under certain conditions, the electron cannot be emitted in the classical direction given by the radiation field.

Atomic untis are used unless otherwise explicitly stated.

2. Theoretical methods

In this section, the theoretical methods employed in the previous works are described [7].

Photoionization cross sections have been evaluated in the framework of the dipole and the adiabatic Born-Oppenheimer (BO) approximations. The fully differential photoionization cross section, i.e., differential in both the energy and direction of the ejected electron and the energy and orientation of the residual H_2^+ molecular ion, is given by Dill's formula [9]:

$$\frac{\mathrm{d}\sigma_\alpha^{\mu_0}(\omega)}{\mathrm{d}\Omega_n \mathrm{d}\Omega_e \mathrm{d}\varepsilon} = \frac{4\pi^2\omega}{c} \sum_{\mu_a,\mu_b} \sum_{\ell_a,m_a} \sum_{\ell_b,m_b} i^{(\ell_a-\ell_b)} e^{i(\hat{\sigma}_{\ell_b}(\varepsilon)-\hat{\sigma}_{\ell_a}(\varepsilon))} (-1)^{m_b+\mu_a-\mu_0} T^*_{\alpha\ell_a m_a \mu_a}(\varepsilon) T_{\alpha\ell_b m_b \mu_b}(\varepsilon)$$

$$\times \sum_{L_e} \left[\frac{(2\ell_a+1)(2\ell_b+1)}{(2L_e+1)} \right]^{\frac{1}{2}} C(\ell_a,\ell_b,L_e;-m_a,m_b,M_e) C(\ell_a,\ell_b,L_e;0,0,0) Y_{L_e}^{M_e *}(\theta_e,\phi_e)$$

$$\times \sum_{L_\gamma} \left[\frac{1}{(2L_\gamma+1)} \right]^{\frac{1}{2}} C(1,1,L_\gamma;-\mu_a,\mu_b,M_\gamma) C(1,1,L_\gamma;-\mu_0,\mu_0,0) Y_{L_\gamma}^{M_\gamma}(\theta_n,\phi_n), \quad (2)$$

with $\mu_{a,b} = 0,\pm 1$, $M_\gamma = -\mu_a+\mu_b$, $M_e = -m_a+m_b$, $\ell_a+\ell_b \geq L_e \geq |\ell_a-\ell_b|$ and $2 \geq L_\gamma \geq 0$. In this equation, $\mu_0 = 0$ for linearly polarized light and $\mu_0 = \pm 1$ for circularly polarized light, α denotes the electronic state of the residual molecular ion, $\hbar\omega$ is the photon energy, ε is the photoelectron energy, $\Omega_e = (\theta_e,\phi_e)$ is the photoelectron emission direction in the molecular frame (θ_e and ϕ_e are the polar angles), $\Omega_n = (\theta_n,\phi_n)$ is the polarization direction with respect to the molecular axis z, c is the speed of light, $C(j_1,j_2,j;m_1,m_2,m)$ denotes a Clebsch-Gordan coefficient, Y_L^M is a spherical harmonic, $\hat{\sigma}_\ell(\varepsilon)$ is the Coulomb phase shift and $T_{\alpha\ell m\mu}(\varepsilon)$ is the transition dipole matrix element given by:

$$T_{\alpha\ell m\mu}(\varepsilon) = \int dR \langle \Psi_{g\nu}(\mathbf{r},R)|\mathbf{e}_\mu \cdot \mathbf{D}|\Psi^+_{\alpha\nu_\alpha\ell m\varepsilon}(\mathbf{r},R)\rangle, \quad (3)$$

where $\Psi_{g\nu}$ is the ground molecular state of energy $W_{g\nu}$, $\Psi^+_{\alpha\nu_\alpha\ell m\varepsilon}$ is the final molecular state of energy $W_{\nu_\alpha}+\varepsilon$ representing a molecular ion in the ν_α vibronic state (either dissociative or non

dissociative) and an ionized electron of energy ε and angular momentum ℓm, $\mathbf{r}$ represents the electronic coordinates, R is the internuclear distance, $\mathbf{e}_\mu$ is the photon polarization vector, and $\mathbf{D}$ is either $\sum_i \mathbf{r}_i$ (length gauge) or $(\hbar\omega)^{-1} \sum_i \nabla_i$ (velocity gauge). Energy conservation implies that $W_{g\nu} + \hbar\omega = W_{v_\alpha} + \varepsilon$. Neglecting rotational effects, the wave functions $\Psi_{g\nu}$ and $\Psi^+_{\alpha v_\alpha \ell m \varepsilon}$ are evaluated in the adiabatic (Born-Oppenheimer, BO) approximation

$$\Psi_{nv_n}(\mathbf{r}, R) = R^{-1}\chi_{v_n}(R)\psi_n(\mathbf{r}, R), \tag{4}$$

where ψ_n and χ_{v_n} are the usual electronic and nuclear BO wave functions [10, 11]. For each value of R, the electronic continuum states must satisfy the usual outgoing boundary conditions of electron-molecule scattering.

Integrating equation (2) over one or several differential magnitudes leads to partially differential or total cross sections, each one representing a specific experimental situation [12]. In particular, integrating equation 2 over the solid angle Ω_e, leads to the cross section differential in the nuclear solid angle and in the energy of the ejected electron irrespective of the electron emission direction [12]:

$$\frac{d\sigma^{\mu_0}_\alpha(\omega)}{d\Omega_n d\varepsilon} = \frac{1}{4\pi} \frac{d\sigma^{\mu_0}_\alpha(\omega)}{d\varepsilon}[1 + \beta^{\mu_0}_{\alpha,n}(\varepsilon)P_2(\cos\theta_n)], \tag{5}$$

where P_2 is the Legendre polynomial of order 2, $d\sigma^{\mu_0}_\alpha(\omega)/d\varepsilon$ is the cross section differential in the energy of the ejected electron,

$$\frac{d\sigma^{\mu_0}_\alpha(\omega)}{d\varepsilon} = \frac{4\pi^2\omega}{3c} \sum_{\ell m \mu} |T_{\alpha\ell m\mu}(\varepsilon)|^2, \tag{6}$$

and $\beta^{\mu_0}_{\alpha,n}(\varepsilon)$ is the nuclear asymmetry parameter

$$\beta^{\mu_0}_{\alpha,n}(\varepsilon) = \frac{3\mu_0^2 - 2}{2} \frac{\sum_{\ell m \mu} |T_{\alpha\ell m\mu - M_i}(\varepsilon)|^2[3(m - M_i)^2 - 2]}{\sum_{\ell m \mu} |T_{\alpha\ell m\mu - M_i}(\varepsilon)|^2}, \tag{7}$$

where M_i is the projection of the initial-state angular momentum. As we pointed out before, in this paper, we restrict our study to linearly polarized light, i.e., $\mu_0 = 0$, and to H_2 molecules initially in the ground state $X^1\Sigma^+_g$, i.e., $M_i = 0$. The above equations can also be used to obtain the cross sections differential in the energy of the residual molecular ion (non dissociative case) or the ejected proton (dissociative case) by using the energy conservation relation

$$W_{g\nu} + \hbar\omega = W_{v_\alpha} + \varepsilon \tag{8}$$

that relates ε to W_{v_α}. Since the ground state of H_2 has $^1\Sigma^+_g$ symmetry, the dipole selection rule implies that only continuum states of $^1\Sigma^+_u$ and $^1\Pi_u$ symmetries can be populated. Hence, the cross section given in Eq. (6) can be written as the sum of $^1\Sigma^+_u$ and $^1\Pi_u$ cross sections

$$\frac{d\sigma_\alpha(\omega)}{d\varepsilon} = \frac{d\sigma^\Sigma_\alpha(\omega)}{d\varepsilon} + 2\frac{d\sigma^\Pi_\alpha(\omega)}{d\varepsilon}. \tag{9}$$

In this paper, we will analyze in detail two particular molecular orientations: parallel ($\theta_n = 0$) and perpendicular ($\theta_n = \pi/2$) to the polarization vector. Hence, from Eq. (5), it can be easily

seen that

$$\left.\frac{\mathrm{d}\sigma_\alpha(\omega)}{\mathrm{d}\varepsilon}\right|_{\theta_n=0} = \frac{\pi\omega}{c}\sum_\ell |T_{\alpha\ell 00}(\varepsilon)|^2 \equiv \frac{1}{4\pi}\frac{\mathrm{d}\sigma_\alpha^\Sigma(\omega)}{\mathrm{d}\varepsilon}$$

(10)

and

$$\left.\frac{\mathrm{d}\sigma_\alpha(\omega)}{\mathrm{d}\varepsilon}\right|_{\theta_n=\frac{\pi}{2}} = \frac{\pi\omega}{c}\sum_\ell |T_{\alpha\ell 11}(\varepsilon)|^2 \equiv \frac{1}{4\pi}\frac{\mathrm{d}\sigma_\alpha^\Pi(\omega)}{\mathrm{d}\varepsilon}.$$

(11)

Summation (integration) in Eqs. (9), (10) and (11) over the energy of the ejected electron when the ionized molecule if left in a non dissociative (dissociative) state leads to the integrated cross section

$$\sigma_\alpha(\omega) \equiv \sum\!\!\!\!\!\int \mathrm{d}\varepsilon \frac{\mathrm{d}\sigma_\alpha^{\mu_0}(\omega)}{\mathrm{d}\varepsilon} = \sigma_\alpha^\Sigma(\omega) + 2\sigma_\alpha^\Pi(\omega)$$

(12)

and the corresponding ones for molecules oriented parallel and perpendicular to the polarization vector, respectively,

$$\sigma_\alpha(\omega)|_{\theta_n=0} = \frac{1}{4\pi}\sigma_\alpha^\Sigma(\omega)$$

(13)

and

$$\sigma_\alpha(\omega)|_{\theta_n=\frac{\pi}{2}} = \frac{1}{4\pi}\sigma_\alpha^\Pi(\omega).$$

(14)

The total photoionization cross section is obtained by summing over all open channels α the integrated cross sections given in Eq. (12):

$$\sigma(\omega) = \sum_\alpha \sigma_\alpha(\omega).$$

(15)

Starting again from equation (2), one can integrate over the solid angle Ω_n to obtain the cross section differential in the energy and solid angle of the ejected electron irrespective of the molecular orientation [13, 14]:

$$\frac{\mathrm{d}\sigma_\alpha^{\mu_0}(\omega)}{\mathrm{d}\Omega_e \mathrm{d}\varepsilon} = \frac{1}{4\pi}\frac{\mathrm{d}\sigma_\alpha^{\mu_0}(\omega)}{\mathrm{d}\varepsilon}[1 + \beta_{\alpha,e}^{\mu_0}(\varepsilon)P_2(\cos\theta_e)],$$

(16)

where $\mathrm{d}\sigma_\alpha^{\mu_0}(\omega)/\mathrm{d}\varepsilon$ is the cross section differential in the energy of the ejected electron given in Eq. (6) and $\beta_{\alpha,e}^{\mu_0}(\varepsilon)$ is the electron asymmetry parameter

$$\begin{aligned}
\beta_{\alpha,e}^{\mu_0}(\varepsilon) =&\ \frac{1}{5}\frac{C(1,1,2;-\mu_0,\mu_0,0)}{\sum_{\ell m\mu}|T_{\alpha\ell m\mu}(\varepsilon)|^2}\sum_{\mu_a,\mu_b}\sum_{\ell_a,m_a}\sum_{\ell_b,m_b}i^{(\ell_a-\ell_b)}e^{i(\hat\sigma_{\ell_a}(\varepsilon)-\hat\sigma_{\ell_b}(\varepsilon))}(-1)^{m_b+\mu_a}\\
&\times\ T_{\alpha\ell_a m_a\mu_a}^*(\varepsilon)T_{\alpha\ell_b m_b\mu_b}(\varepsilon)\\
&\times\ [(2\ell_a+1)(2\ell_b+1)]^{\frac{1}{2}}C(\ell_a,\ell_b,2;-m_a,m_b,M_e)C(\ell_a,\ell_b,2;0,0,0)C(1,1,2;-\mu_a,\mu_b,M_\gamma)\\
&\times\ \delta_{m_a+\mu_a,m_b+\mu_b}.
\end{aligned}$$

(17)

The evaluation of the wave functions involved in the $T_{\alpha \ell m \mu}$ matrix elements requires the use of computational techniques. It is worthy to be mentioned that such techniques have been employed with succes to analyze many ionization reactions of H_2 targets. Among them, we cite resonant dissociative photoionization [11, 15, 16] and ion impact ionization [17]. Moreover, they allowed the obtention of the first numerical solution of the complete photo-induced break-up of H_2 [18]. More specifically, the vibrational (bound and dissociative) wave functions have been expanded in a basis of 280 B-splines of order $k = 8$ contained in a box of 12 a.u.. The electronic wave functions have been evaluated as described in detail in Refs. [10, 11]. Briefly, the ground state Ψ_g results from a configuration interaction (CI) calculation in which the H_2 hamiltonian has been diagonalized in a basis of 321 configurations built from products of one-electron H_2^+ orbitals and pseudo-orbitals. The calculated energy at the equilibrium internuclear distance is -1.8865023 a.u., to be compared with the exact non relativistic value -1.88876138 a.u. [19]. All these orbitals have been represented through a one-center expansion that includes spherical harmonics up to $\ell = 16$. The corresponding radial parts have been expanded in a basis of 310 B-splines of order $k = 8$ in a box of radial length of 60 a.u.. The final electronic continuum state $\Psi^+_{\alpha v_\alpha \ell m \varepsilon}$ results from a close coupling calculation that includes all partial waves with $\ell \leq 7$ associated with the four lowest ionization thresholds of H_2: $X^2\Sigma_g^+$ $(1s\sigma_g)$, $^2\Sigma_u^+$ $(2p\sigma_u)$, $^2\Pi_u$ $(2p\pi_u)$, and $^2\Sigma_g^+$ $(2s\sigma_g)$. For every value of R, these continuum states satisfy the usual boundary conditions corresponding to (i) one electron in a bound electronic state of H_2^+ and (ii) the other electron in a single outgoing spherical wave with a well defined value of the angular momentum ℓ plus a combination of incoming spherical waves for all accessible electronic states of H_2^+ and all possible values of the angular momentum of the ejected electron compatible with the molecular symmetry [10] (At the photon energy considered in this work, for a given energy, there is always a continuum state for each electronic state α of the residual H_2^+ ion and angular momentum ℓ of the ionized electron).

In this way, we represent in a realistic way the molecular nature including electron correlation and the two-center character of the molecular potential in all bound and continuum wavefunctions. Moreover, interferences among the various ionization thresholds and angular momenta of the ejected electron was taken into account through $\Psi^+_{\alpha v_\alpha \ell m \varepsilon}$. The convergence of the close coupling expansion was verified by performing calculations (for a reduced number of photon energies) in which six additional ionization thresholds were considered [6]. Those tests do not exhibit relevant variations in the dominant channel, i.e., the $^2\Sigma_g^+ (1s\sigma_g)$ one.

3. Results

3.1. Validity of the Cohen and Fano model

To analyze the validity of equation (1), we calculated cross sections ratios dividing H_2 results by twice the ones of atomic H [6]. The result is shown in Fig. 1 as a function of photon energy.

Strong oscillations are clearly visible in both 4- and 10-channel calculations. We include also in Fig. 1 a fitting to the Cohen-Fano formula (1), leaving $a_0 = \sigma_H/(1 + S)$ and $a_1 = R$ as free parameters. The fit produces $a_0 = 1.46$ and $a_1 = 1.57$. At high photon energies, the fitting backs the Cohen-Fano model. Extensions of this model have been proposed to interpret similar oscillatory behaviours observed in ionization of D_2 by fast heavy ions [3] and electrons [4]. As in the Cohen-Fano model [2], these theories are based on a one-electron description of ionization and an LCAO representation of the initial molecular state. This has led to results in reasonable agreement with experiments for large k_e. However, none of these theories have been able to reproduce the fall of the experimental $\sigma/2\sigma_H$ ratio when k_e decreases (see Fig. 1). The present results do show such a fall, in excellent agreement with the measurements of Samson and Haddad [23] (see Fig. 1). This is the first theoretical evidence of these observations.

The failure to reproduce the observed behaviour at relatively low photon energies using the fitting function given in equation (1) indicates that at least one of the basic assumptions of the
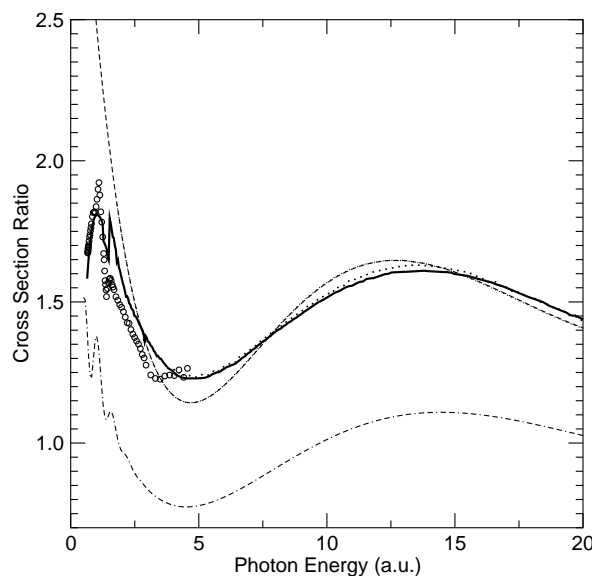
Figure 1. The $\sigma_{H_2}/2\sigma_H$ photoionization ratio. 4-channel (full line) and 10-channel (dotted line) results. Circles, experiments by Samson and Haddad taken from [20] and divided by $2\sigma_H$. Dashed line, fit of $\sigma_{H_2}/2\sigma_H$ to the Cohen-Fano formula (1) (see text). Results for a fictitious one electron molecule (dashed and dotted line); for the sake of clarity, the curve has been multiplied by 0.25 (see text for details).

Cohen-Fano model does not hold. To clarify this fact, we show in Fig. 1 B-spline results for a *fictitious* one-electron diatomic molecule with nuclear charges $Z = 0.5$ and equilibrium distance $R = 1.4$ au. This system differs from the real H_2 molecule in the absence of correlation and screening whereas all the other aspects are treated as in H_2. At high electron energies, this model calculation reproduces qualitatively those of H_2 but at lower energies it fails to reproduce the fall of the $\sigma/2\sigma_H$ ratio. Therefore, the origin of this fall must be electron correlation and/or screening. Indeed, at low k_e, the ejected electron is more sensitive to details of the potential near the nuclei. In particular, in a real H_2 molecule, a slow electron feels a charge larger than 0.5 due to incomplete screening of the inner electron, which must lead to a decrease of the ionization cross section. Electron correlation is expected to play a significant role only in the vicinity of the doubly excited states of H_2, where the nuclear motion cannot be neglected. Fig. 1 shows some structure near the ionization threshold on the curve of the fictitious one-electron molecule.
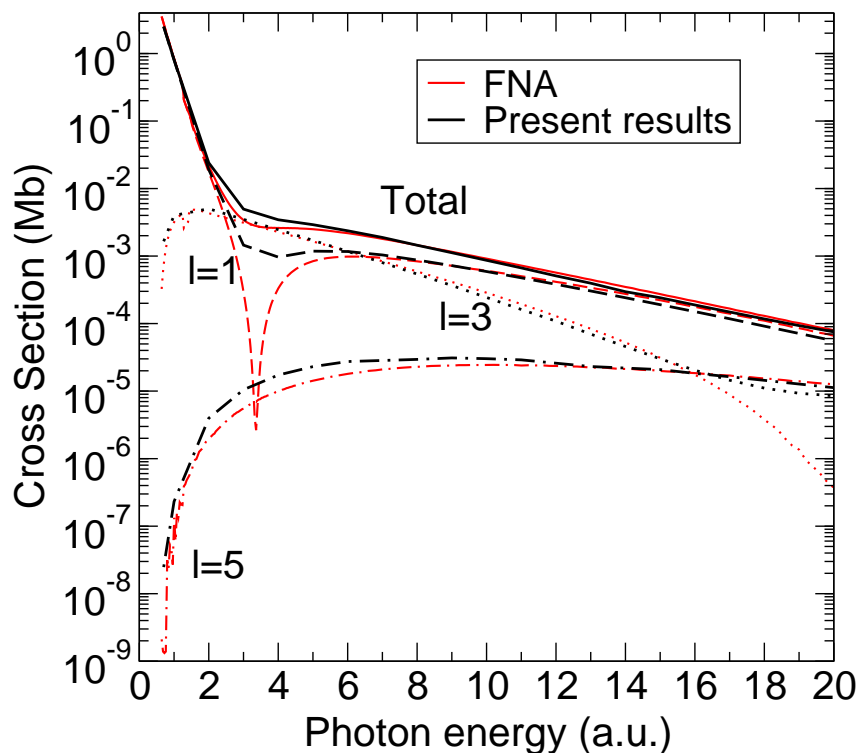
Figure 2. (Color online) Partial wave contributions to the H_2 photoionization cross section associated with the $^2\Sigma_g^+(1s\sigma_g)$ ionization threshold. Results for $^1\Sigma_u^+$ symmetry. Results from the FNA are shown by red curves.

This is probably provoked by the two-centre nature of the electronic continuum that is absent in the Cohen-Fano model but must be visible for electrons with small kinetic energy.

3.2. Confinement effects

In Fig. 2, we show results for the different partial waves associated with the lowest ionization channel $^2\Sigma_u^+(1s\sigma_g)$ for the $^1\Sigma_u^+$. It can be seen that results including the nuclear motion do differ significantly from the FNA ones [6]. Discrepancies are more evident at photon energies of ~ 3.5 a.u. and > 20 a.u. where the $\ell = 1$ and $\ell = 3$ partial waves contributions exhibit a minimum, respectively. Analogous minima were observed for FNA results for the case of H_2^+ [21]. For photon energies around 3.5 a.u., it can be seen from 2 that the minimum observed for the $\ell = 1$ wave in the H_2 FNA results is more pronounced than in calculations including the nuclear motion. On the contrary, its position is only slighlty changed by the nuclear motion. As shown in our previous work [8], such minima are expected to appear when the momentum of the ejected electron satisfies the condition:

$$k_e R_e \sim \ell\pi \quad (\ell = 2n + 1) \tag{18}$$

where k_e and R_e are the ejected electron momentum and the equilibrium internuclear distance, respectively. The condition requires that the product $k_e R_e$ be equal to an odd number times π. Incidentally, the l angular momenta associated to the partial waves used in the description of the final continuum states must be also odd due to the symmetry requirements imposed by the selection rules. So, we use these odd l values to express the mentioned condition.
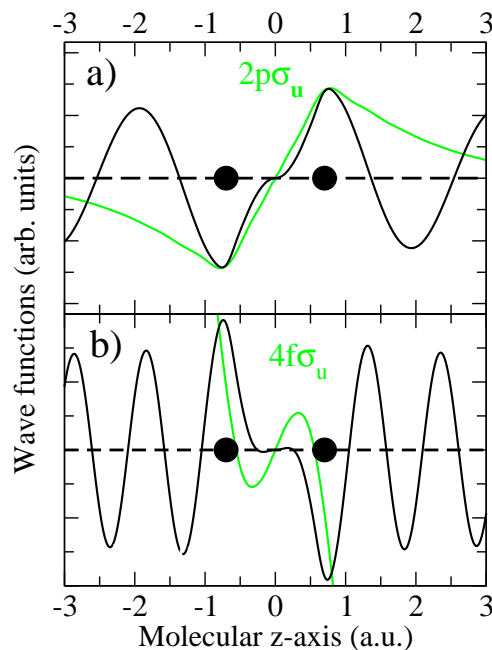
Figure 3. (Color online) Wave functions of the ejected electron (black line) compared with the lowest H_2^+ molecular orbitals (green line) along the internuclear z-axis for the k and ℓ values satisfying approximately the confinement condition. The wave functions of the ejected electron, obtained at the equilibrium distance, are the real K-matrix standing waves that correspond to the calculated complex S-matrix scattering wave functions. Panel a, $\varepsilon = 2.6$ a.u. and $\ell = 1$; panel b, $\varepsilon = 19$ a.u. and $\ell = 3$.

According to this simple formula, the minimum in the $\ell = 1$ partial wave should appear at a photon energy of ~ 3.1 a.u. and that of the $\ell = 3$ one at ~ 23 a.u.. These values are in reasonable agreement with the actual ones observed in Fig. 2.

The electron energies, $\varepsilon = k_e^2/2$, obtained by using Eq. 18 are the same as the ones of an electron confined in a one-dimensional infinite-square well potential of width R_e. This coincidence inspired us the word 'confinement' to refer to this interference effect. In fact, for the particular k_e values given by Eq. 18, a system of standing waves is created in the inner region $|r| < R_e$ leading to destructive interferences outside this region and producing consequently no propagating waves. At high energies, the minima location is also the one found in the transmission function for a one-dimensional potential made of two delta functions separated by a distance R_e. The $k_e R_e = \ell\pi$ condition obtained from these two models where $l = 2n + 1$ indicates an odd number (of course, in all these analogies, l is not any angular momentum, it is just an odd number) can be easily understood considering that in three dimensions (a real situation), the electrons tend to move in the directions given by the electric field of the incident radiation. As shown by Eq. (13), the $^1\Sigma_u^+$ cross section represents photoionization of H_2 molecules oriented parallel to the polarization axis, then electrons are mostly forced to move along the internuclear axis. Owing to the fact that the ejected electron has a large kinetic energy, it will only be affected by the potential in the vicinity of the two nuclei, which is similar to what happens in a one-dimensional infinite-square well or in the scattering by two delta functions. Hence the larger k_e the more accurate the formula $k_e R_e \sim \ell\pi$. This is indeed what happens in H_2 photoionization even for the lowest value of k_e that arise from this formula ($\ell = 1$) and also, as shown in [6] and [24], in H_2^+ photoionization.
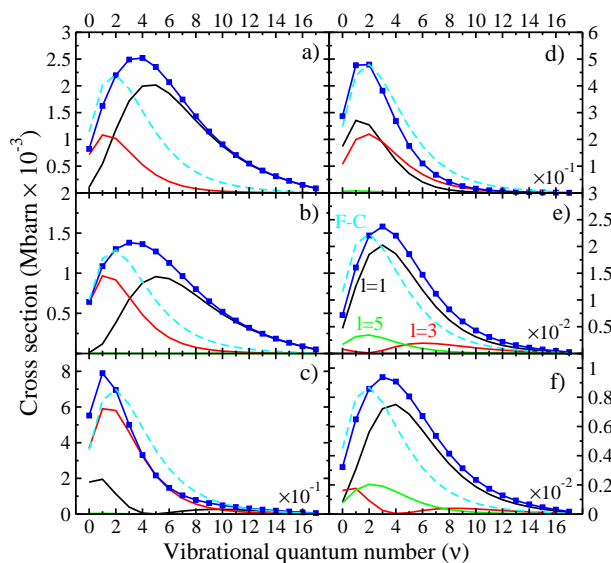
Figure 4. (Color online) Non dissociative photoionization cross section of H_2 of $^1\Sigma_u^+$ symmetry, as a function of the vibrational quantum number v of the residual H_2^+ ion at photon energies 2, 2.5, 3.5, 6.0, 16.5 and 20 a.u., panels a, b, c, d, e and f, respectively. Blue line with squares, total cross section; black line, $\ell = 1$ partial wave contribution; red line, $\ell = 3$; green line, $\ell = 5$. Dashed cyan line, Frank-Condon distribution (FC).

In Fig. 3, it can be seen that the reduced electron continuum wave function at $R_e = 1.4$ a.u (the equilibrium internuclear distance of H_2) associated with the $\ell = 1$ partial wave is very similar in fashion to the $2p\sigma_u$ orbital of H_2^+ (with $R_e = 2$ a.u.) in the region between both molecular centers. In turn, the reduced continuum wave function associated with the $\ell = 3$ partial wave has the same nodal structure as the $4p\sigma_u$ orbital in between the nuclei. This similarity between reduced electron continuum waves and the H_2^+ molecular orbitals gives additional evidence for the image of partial-wave confinement. In Ref. [24], the minima in the $^1\Sigma_u^+$ cross section have been interpreted as Cooper-like minima similar to those found in atomic photoionization. The continuum wave functions of H_2^+ were unfortunately compared with the $1s\sigma_g$ orbital, which does not have the correct nodal symmetry imposed by the dipole selection rule. Moreover, this interpretation does not bring a simple prediction for the minima as the one given by our Eq. 18.

3.3. Non Franck-Condon effects
In what follows, we consider only non dissociative photoionization that is the most important contribution to the total cross section.

At low photon energies (e.g., 20 eV), the vibrational distribution of residual H_2^+ follows approximately a Franck-Condon distribution, which predicts that the $v = 2, 3$ vibrational levels should be the most populated ones.

In Fig. 4 we show cross sections differential in the vibrational energy of the residual H_2^+ ion (viz. the reverse of the energy of the ejected electron) for the non dissociative case and for both parallel ($^1\Sigma_u^+$) molecular orientations.

It can be seen that the population of the final vibrational states does not follow a Franck-Condon behavior, even for a photon energy of 2 a.u.. At this energy, the $\ell = 1$ partial wave is dominant for almost all v, but, surprisingly, the $\ell = 3$ partial wave dominates for the lowest v's. As the photon energy increases reaching the region in which the $\ell = 1$ partial wave has a
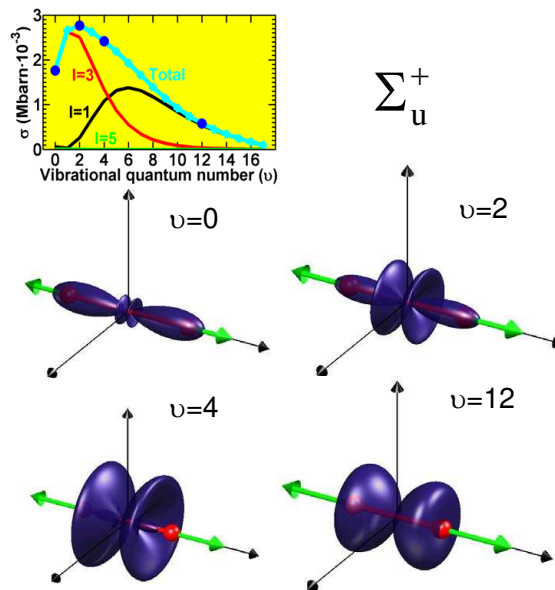
Figure 5. (Color online) Electron angular distributions for non-dissociative photoionization $(H_2 + \hbar\omega \rightarrow H_2^+(v) + e^-)$ of H_2 oriented parallel (Σ_u^+ symmetry) to the polarization direction at a photon energy of 2.5 a.u.. Angular distributions corresponding to leaving the residual H_2^+ ion in different vibrational states are shown by three dimensional plots in blue. For a better visualization, these distributions have been renormalized so that their maximum value is always 1. The polarization direction is indicated by the double arrow (green). The two nuclei are indicated by two small spheres (red). The angle-integrated cross sections, including the partial wave decomposition, as a function of the final quantum vibrational number v are shown in the two-dimensional plots.

minimum (see Fig. 2), the $\ell = 3$ partial wave becomes dominant at higher and higher v until, at energies above 6 a.u., the $\ell = 1$ partial wave becomes again the dominant one. A more careful inspection of Fig. 4 shows that the $\ell = 1$ partial wave has a minimum around $v = 5$ at a photon energy of 3.5 a.u.. This is a photon energy that lies in the minimum of the cross section (see Fig. 2). Another minimum is clearly visible for the $\ell = 5$ partial wave at photon energies of 16.5 and 20 a.u but now located around $\nu = 4$. From this analysis one may conclude that this deviation from the FC predictions is related to the confinement effects discussed above.

3.4. Interference effects in the angular distribution of electrons

For the perpendicular orientation, one can see that the electronic emission is mainly produced, as expected, in the direction of the polarization vector. As the photon energy increases, additional lobes appear producing interference patterns analogous to the ones of the Young's double-slit experiment given by $R \sin \theta_e = n\lambda_e$ [8].

In Fig. 5, we show the electron angular distributions for non-dissociative photoionization of H_2 for molecules parallel (Σ_u^+ symmetry) to the polarization direction at a photon energy of 2.5 a.u.. The corresponding angular distributions are only shown for the case of H_2^+ ions left in the $v = 0, 2, 4,$ and 12 vibrational levels. The first three values of v correspond to vibrational levels that are close to or within the FC region, while the $v = 12$ vibrational level is clearly outside this region. The distribution has an almost perfect f shape ($\ell = 3$) when H_2^+ remains in a low vibrational level. As the vibrational quantum number of the remaining H_2^+ increases,

a complicated angular pattern emerges as the result of the interference between the $\ell = 1$ and $\ell = 3$ partial waves. For $\upsilon = 4$, interferences lead to almost no emission in the direction of the polarization vector, whereas, for $\upsilon = 12$, the distribution is almost p-like. In Ref. [8], this sudden change of the angular distribution with υ has been attributed to confinement because, around this photon energy, the $\ell = 1$ partial component of the $^1\Sigma_u^+$ integrated cross section exhibits a pronounced minimum (see Fig. 2).

In the case of H_2^+ photoionization, the angular distributions approximately follow the formula [25] $(\mathbf{e}_\mu \cdot \mathbf{k}_e)^2 \cos^2(\mathbf{k}_e \cdot \mathbf{R}/2)$. If $\mathbf{e}_\mu$ and $\mathbf{k}_e$ are parallel to the molecular axis, this formula leads to zero when $k_e R = \pi, 3\pi, ...$, i.e., no electron emission along the molecular axis in agreement with the image of confinement.

4. Conclusions

Photoionization of H_2 ionization by photons of a few hundred eV has been studied. By using B-spline functions to evaluate bound and continuum states and within the framework of the Born-Oppenheimer approximation, we obtain a realistic description of the molecular sates including its nuclear degrees of freedom.

The Cohen and Fano predictions were analyzed showing that they are valid at sufficiently high photon energies. Failures are related to electronic correlation and/or screening [6].

In the case of molecules oriented parallel to the polarization direction, the partial-wave cross sections exhibit pronounced minima at electron energies determined closely by $k_e R_e = \ell\pi$, where ℓ is an odd number and R_e is the equilibrium internuclear distance [7, 8].

The fully differential angular distribution presents in a clear way the effects of confinement for molecules aligned parallel to the polarization direction. Young's double slit interferences are clearly visible in the perpendicular case when the electron wavelength is comparable to the internuclear distance [7, 8] .

From the analysis of the vibrational distribution of the residual H_2^+ ion for the dominant non-dissociative channel, it is found that molecules parallel to the polarization direction transitions do not follow the typical Franck Condon (FC) distribution. Deviations from the FC distribution are more pronounced in the regions where confinement occurs. On the contrary, no deviations are observed for molecules perpendicular to the polarization direction [7].

References

[1] D. Akoury *et al*, *Science* **318** (2007) 949.
[2] Cohen H D and Fano U 1966 *Phys. Rev.* **150** 30
[3] Stolterfoht *et al* 2001 *Phys. Rev. Lett.* **87** 023201
[4] O. Kamalou, J.-Y. Chesnel, D. Martina, F. Frémont, J. Hanssen, C. R. Stia, O. A. Fojón, R. D. Rivarola 2005 *Phys. Rev. A* **71** 010702(R).
[5] S. Chatterjee, S. Kasthurirangan, A. H. Kelkar, C. R. Stia, O. A. Fojón, R. D. Rivarola, and L. C. Tribedi 2009 *J Phys. B: At. Mol. Opt. Phys.* **42** 065201

[6] O. A. Fojón, J. Fernández, A. Palacios, R. D. Rivarola, F. Martín 2004 *J. Phys. B: At. Mol. Opt. Phys.* **37** 3035.

[7] J. Fernández, O. A. Fojón and F.Martín 2009 *Phys. Rev. A* **79** 023420

[8] J. Fernández, O. A. Fojón, A. Palacios, and F. Martín 2007 *Phys. Rev. Lett.* **98** 043005

[9] Dill D 1976 *J. Chem. Phys.* **65** 1130

[10] Martín F 1999 *J. Phys. B: At. Mol. Opt. Phys.* **32** R197

[11] Bachau H, Cormier E, Decleva P, Hansen J E and Martín F 2001 *Rep. Prog. Phys.* **64** 1815

[12] S. Wallace and D. Dill 1978 *Phys. Rev. B* **17** 1692 .

[13] J. C. Tully, R. S. Berry, and B. J. Dalton 1968 *Phys. Rev.* **176** 95

[14] I. Cacelli, V. Carravetta, A. Rizzo, and R. Moccia 1991 *Phys. Rep.* **205** 283

[15] I. Sánchez and F. Martín 1999 *Phys. Rev. Lett.* **82** 3775

[16] F. Martín et al. 2007 *Science* **315** 629

[17] Laurent, Fernández, Legendre, Tarisien, Adoui, Cassimi, Fléchard, Frémont, Gervais, Giglio et al. F 2006 *Phys. Rev. Lett.* **96** 173201

[18] Vanroose, Martín, Rescigno, and McCurdy 2005 *Science* **310** 1787

[19] Kolos W, Szalewicz K and Monkhorst H J 1986 *J. Chem. Phys.* **84** 3278

[20] Chung Y M, Lee E M, Masuoka T and Samson J A R 1993 *J. Chem. Phys.* **99** 885

[21] O. A. Fojón, A. Palacios, J. Fernández, R. D. Rivarola, and F.Martín 2006 *Phys. Lett. A* **350** 371

[22] F. Martín 1999 *J. Phys. B: At. Mol. Opt. Phys.* **32** R197

[23] Samson J A R and Haddad G N 1994 *J. Opt. Soc. Am. B* **11** 277

[24] R. Della Picca, P. D. Fainstein, M. L. Martiarena, and A. Dubois 2008 *Phys. Rev. A* **77** 022702

[25] Walter M and Briggs J 1999 *J. Phys. B: At. Mol. Opt. Phys.* **32** 2487